RESEARCH SIGNPOST

Research Signpost
37/661 (2), Fort P.O., Trivandrum-695 023, Kerala, India

Recent Res. Devel. Mat. Sci., 3 (2002): 633-662 ISBN: 81-7736-141-4

Vapor phase preparation and some properties of carbon micro-coils/nano-coils

S. Motojima[1], Y. Hishikawa[2] and H. Iwanaga[3]

[1]Department of Applied Chemistry, Faculty of Engineering, Gifu University, Gifu 501-1193, Japan
[2]CMC Technology Development Co. Ltd., Sue-cho, Kakamigahara-shi, Gifu 509-0108, Japan
[3]Department of Materials Technology, Faculty of Engineering, Nagasaki University
Nagasaki 852-8131, Japan

Abstract

Carbon micro-coils is a novel functional materials with helical/spiral forms with a coil diameter of μm~nm orders, and a possible candidate for electromagnetic absorbers, hydrogen absorber, field emitter, tunable micro devices, micro sensors, chiral catalyst, capacitors, energy convertors, etc. We have obtained the carbon micro-coils with a coil diameter of μm~nm orders by the metal-catalyzed pyrolysis of acetylene. In this review, the preparation conditions, morphology, growth mechanism, and some properties of the carbon coils are introduced. The most optimum preparation conditions for obtaining the carbon coils are as follows; carbon source: acetylene, catalyst: Ni fine powder, Impurity: H_2S, reaction temperature: 750~800°C. Various energy fields, such as electromagnetic,

Correspondence/Reprint request: Dr. S. Motojima, Department of Applied Chemistry, Faculty of Engineering, Gifu University, Gifu 5011-1193, Japan. E-mail: motojima@apchem.gifu-u.ac.jp

magnetic, ultrasonic, plasma fields, etc., accelerate the growth of carbon coils and strongly affects on the morphology and some physical properties. The as-grown carbon micro-coils have almost amorphous structure, but is graphitized by high temperature heat treatment under full preservation of the coiling morphology. The graphite micro-coils have a "herring-bone structure". The micro-coils or micro-tubes of various transition metal carbides and nitrides can be obtained by the vapor phase metalizing and/or nitriding of the carbon coils with full preservation of the coiling morphology. The carbon coil shows the excellent electromagnetic absorption and field emission properties.

1. Introduction

As can be seen in the great maelstrom of the cosmos, the ∝-helix of proteins, double helix of deoxynucleic acid (DNA), or screw dislocation in solids, the three-dimensional (3D) helical/spiral structure is the fundamental structure of all objects. Materials with bulk, plate, thin films, powder, or straight fiber-like morphologies are now commonly available. However, materials with the 3D-helical/spiral structures have never been commercially available. Many researches have been trying to prepare the materials with a 3D-helical/spiral structure. Davis el al. was the first report the vapor growth of thin carbon fibers twisted together in the form of a rope (1). After then, the vapor phase preparation of micro-coiled fibers, such as carbon(2-5), SiC(6-8), Si_3N_4(9-12), BN(13), B(14), etc. have been reported. Recently, the vapor growth and structure of helical-coiled carbon nanotubes or nanofibers are also reported (15-22). However, the growth of these micro/nano-coiled fibers is mostly accidental and the reproducibility is very poor. Ihara et al. have demonstrated the possible presence of the high-order fullerenes (C_{360}~C_{2160}) with helically coiled forms by the molecular dynamic simulations, and presented the semi-metallic and novel functional characteristics which could not be obtained by common materials (23). Pan et al. reported that carbon tubule nanocoils have excellent field emission properties (24). Materials with such singular helical/spiral structures are potential candidates such as absorbers of electromagnetic waves, tunable microelectronic devices, microsensors, electron emitter, electric double layer capacitor, hydrogen storage materials, catalyst, chiral mold, etc.

We have prepared regularly micro-coiled carbon fibers by the catalytic pyrolysis of acetylene containing a small amount of sulfur or phosphorus impurity at 750-800 °C(25-37). The micro-coiled carbon fibers have a 3D double helical /spiral structure. Accordingly, we named these micro-coiled carbon fibers "cosmo-mimetic carbon micro-coils" (referred to as "carbon coils" hereafter) after "bio-mimetic materials" (38).

In this review, the vapor phase preparation conditions, morphology, growth mechanism and some properties of the carbon coils are introduced, and the potential applications is discussed.

2. Experimental

Fig. 1 shows the schematic apparatus used for the preparation of carbon coils. A graphite plate, on which catalyst (powder or thin film) was supported, was used as the

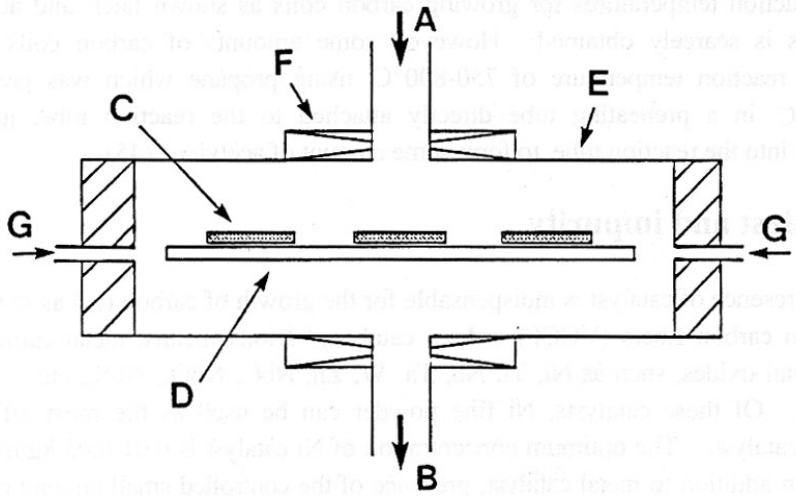

Figure 1. Schematic apparatus.
A)Source gas inlets (C_2H_2+H_2+ impurity), B)Gas outlet, C) substrate (graphite plate), D) susceptor, E) reaction tube (quartz, 100mm i.d. x 1000mm long), F) heater, G) N_2

substrate, and was set in the horizontal reaction tube (quartz, 1000mm length, 100 mm i.d.). Metal fine powder (0.05~5 mμm diam.) used as a catalyst was dispensed by smearing with concentration of about 0.02 kg/m^2-substrate on the substrate surface. The reaction tube was heated from the outside by electric heater using AC or DC, or by propane gas burner. A gas mixture of C_2H_2+H_2+N_2+ impuirty was vertically introduced onto the substrate surface and exhausted through the lower gas outlets. The standard reaction conditions used are as follows: reaction temperature=750-800°C, gas flow rate of acetylene=150-200 sccm, impurity (thiophene) content in total gases=0.6-0.8 vol.%, gas flow ratio (H_2/C_2H_2)=3-4. Fine powder or sputtered thin films of Ni, Au, Pt, Fe, etc. were used as a catalyst.

3. Preparation conditions

3.1. Carbon source

As a carbon source, acetylene was the most effective one for the preparation of carbon coils. Baker et al. also obtained carbon coils using acetylene as the carbon source (39-40). Many carbon compounds other than acetylene, such as CO (41), methane (42), ethylene (43-44), propylene (43), propane (45), 1-butene (43), cis-2-butene (43), and allene (4) were also used as the carbon source. However, when using hydrocarbon other than acetylene, the carbon coils were rarely obtained under any reaction conditions. Hydrocarbons usually catalytic decomposes to form some amounts of acetylene, which are effectively available for growing carbon coils. When propane undergoes catalyzed pyrolysis, acetylene is formed at 900~1100 °C (46-48). However, acetylene is not formed at 750~800 °C, which is the

optimum reaction temperatures for growing carbon coils as shown later, and accordingly carbon coils is scarcely obtained. However, some amounts of carbon coils could be obtained at reaction temperature of 750-800°C using propane which was preheated at 1000-1100°C in a preheating tube directly attached to the reaction tube, just before introduction into the reaction tube, to form some amount of acetylene (45).

3.2. Catalyst and impurity

The presence of catalyst is indispensable for the growth of carbon coil as in the case of vapor grown carbon fibers (VGCF). As a catalyst, various metals, metal carbides, metal sulfides, metal oxides, such as Ni, Ti, Nb, Ta, W, Zn, NbC, NbO_x, NbS_x, etc. can be used (27-29, 49). Of these catalysts, Ni fine powder can be used as the most effective and convenient catalyst. The optimum concentration of Ni catalyst is 0.01-0.03 kg/m^2-substrate surfaces. In addition to metal catalyst, presence of the controlled small amount of sulfur or phosphorus compounds, such as thiophene, H_2S, PH_3, etc. is indispensable for the growth of carbon coils as an impurity (or co-catalyst) in the reaction atmosphere. No carbon coils could be obtained under without or larger amount of these impurities. The optimum concentration of impurity is 0.03~0.05 mol% in total gases for H_2S and PH_3 and 0.5-1.0 mol% for thiophene. Hereafter, Ni catalyst and thiophene impurity were used, unless otherwise noted.

3.3. Temperature and gas flow rate

The optimum reaction temperature was 700~850 °C depending on the kind of catalyst and impurity (27~29). For example, the optimum reaction temperature is 750~800 °C for Ni catalyst and thiophene impurity.

3.4. Effect of application of outer energy field (50,51)

The carbon coils can be absorbed very effectively an electromagnetic wave as will be shown later. Using conventional electric heater, electromagnetic wave (28-33 mG at substrate surface) is irradiated from the electric heater into growing atmosphere of the carbon coils. It was observed that the outer electromagnetic wave (referred to as "EM wave" hereafter), emitted from the outer electric heater, and/or bias voltage strongly influenced on the growth and morphology of the carbon coils. The coil yield obtained with irradiation of EM wave increased by 1.6~2.3 times higher than that without irradiation in which gas burner heater was used. Furthermore, the coils yield obtained with a bias voltage (AC and DC) to the substrate was 2.2~2.3 times higher than that without bias voltage, and the yield increased with increasing bias voltage. Application of magnetic flux from a permanent magnet (~ 0.03 Tesla) to the reaction atmosphere did not increase the coil yield, but influenced on the morphology. The coil yield increased by applying ultrasonic wave (15~45KHz) to the reaction atmosphere. The density of the carbon coils increased by applying energy field of

EM wave, magnetic flux and ultrasonic wave to reaction atmosphere or substrate as shown later.

4. Morphology and growth mechanism

4.1. Deposition patterns

The carbon coil grew perpendicularly on the substrate surface, and the thickness of coil layers reached 4~8 mm thick after 2 hrs reaction time. Figs. 2 and 3 show the cross section of the coil layers deposited on the substrate after 2 hrs reaction time and the enlarged SEM views, respectively. The yield of carbon coils obtained under the optimum conditions was 20~30 mg/cm^2-substrate, and carbon coil of 20-30 g could be obtained for one reaction batch of 2hrs reaction times.

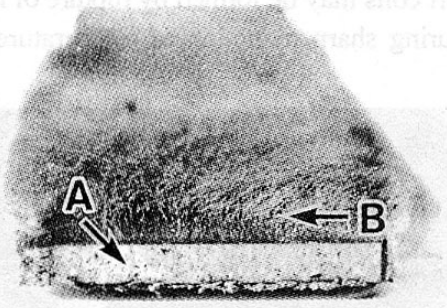

Figure 2. Cross-section of the deposits. A)Graphite substrate, B) carbon coil layers.

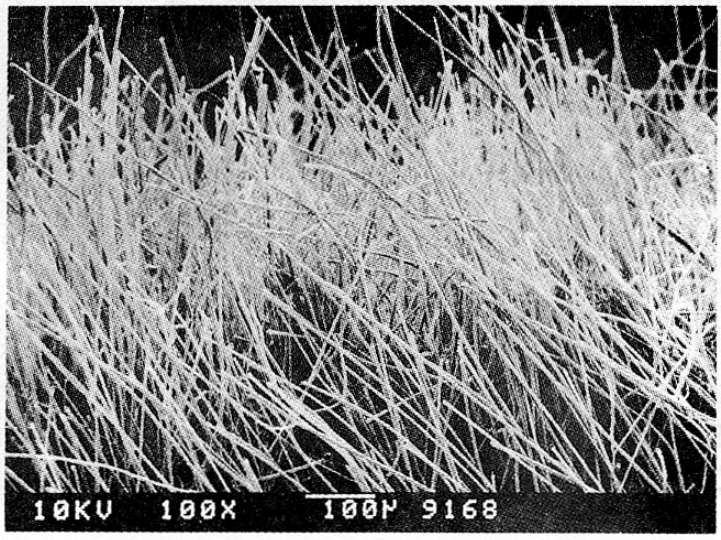

Figure 3. Upper part of the carbon coil layers.

4.2. Morphology

The carbon coil layers grew on the substrate are apparently composed of almost straight fiber forms at low magnification as shown in Fig. 3. However, all of these apparently straight fibers are perfectly coiled without exception. That is, the purity or content of carbon coils in the deposited coil layers was almost 100%. Fig. 4 shows the tip part of the carbon coils obtained using Ni catalyst. The carbon coils grew perpendicularly, pointing in the direction of the source gas inlets, on the graphite substrate as shown already in Figs. 2 and 3. A fine Ni grain material used as a catalyst was always observed on the tip part of all of carbon coils (arrow in Fig. 4). The micro-coiling morphology is formed by the rotation of a Ni catalyst grain that is exclusive growing point for carbon coils. The coiling (rotating) speed is about one cycle per second around the coil axis. The hard carbon layers of 0.3~0.8 mm thick, on which carbon coil layer grew, were commonly deposited between substrate surface and coil layers. Between the hard carbon layers and bottom part of the carbon coil layers, ruptured short coils of 50~300μm long were commonly observed as shown in Fig. 5. These short coils may be formed by rupture of long carbon coils caused by large inner stress formed during sharp reduction of temperature at stopping the reaction.

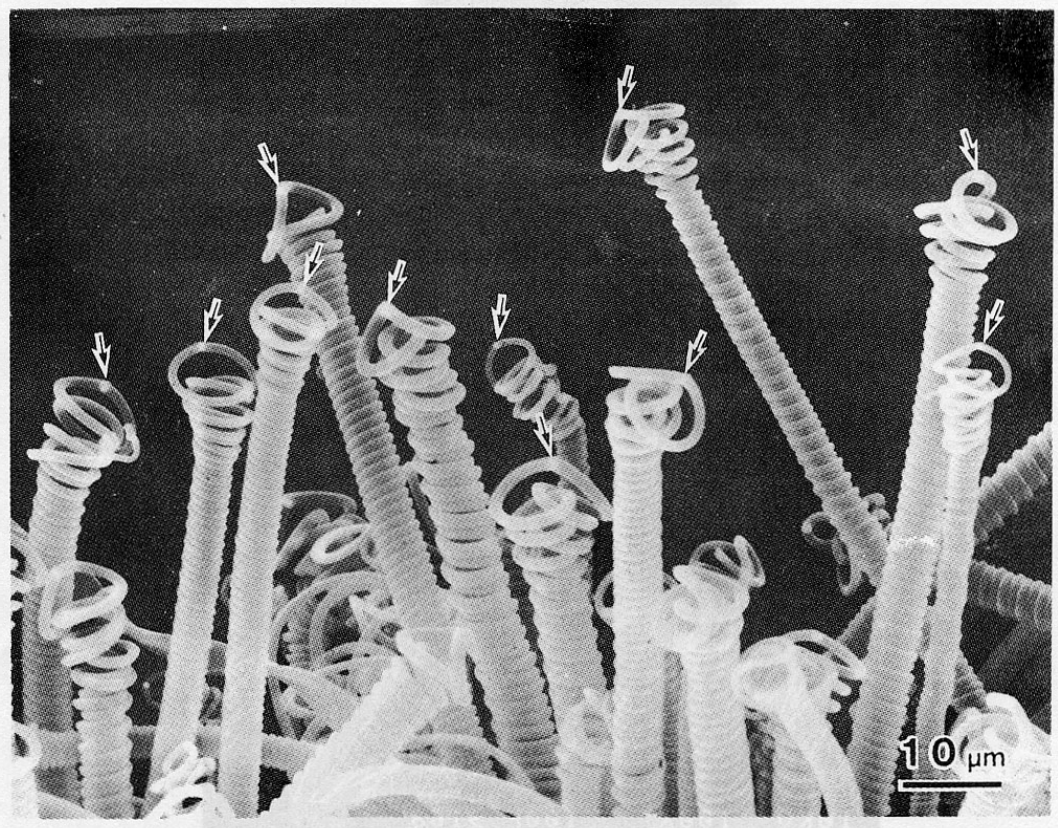

Figure 4. The enlarged view of the tip part of the carbon coils. Reaction time: 5 min. Arrow indicates a catalyst grain.

The carbon coils with various coiling morphology; regular coils, irregular coils, double coils, single coils, etc. can be obtained depending on the reaction conditions. Fig. 6 shows a representative regular-coiled carbon coil. This regular coil have a constant coil diameter of 2.6μm and coil pitch of 0.4μm without any coil gap throughout one coil. The cross section of the fiber, which formed of a carbon coil, is circular or elliptical-forms. We call these coils as "circular-coils" hereafter. Another type of regular coil is shown in Fig. 7, in which cross

Figure 5. Ruptured short coils observed on the bottom part of the coil layers.

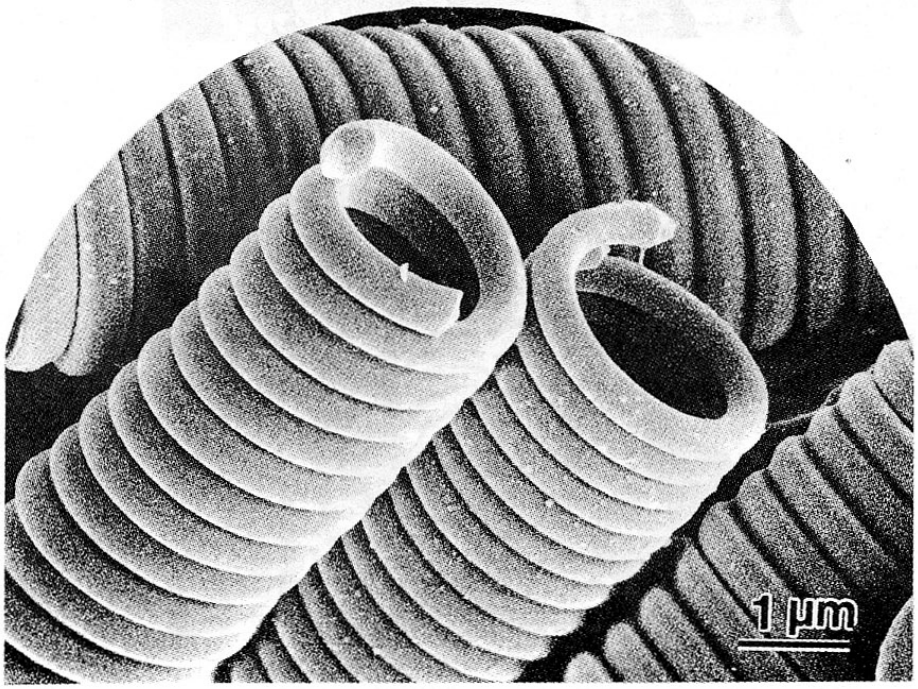

Figure 6. Regular carbon coils ("circular coils").

section of the fiber is rectangular or ribbon-like-forms, and we call these coils as "flat coils" hereafter. The coil diameter and coil pitch of the regular carbon coils have a constant value from micrometer to nanometer orders throughout a piece of carbon coils. Fig. 8 shows irregular-coiled carbon coils with various coil diameter and coil pitch. The coil length reaches to 5~10 mm long for 2 hrs reaction time.

Almost all of the carbon coils are double-coiled forms in which two fibers entwine with each other such as the double helix of a DNA as can be seen in Fig. 6. The amount of carbon coils having right- and left-clockwise coiled forms are about the same. Sometimes, the carbon coils with various interesting and artistic coiling morphology can be seen. Fig. 9

Figure 7. Regular carbon coils ("flat coils").

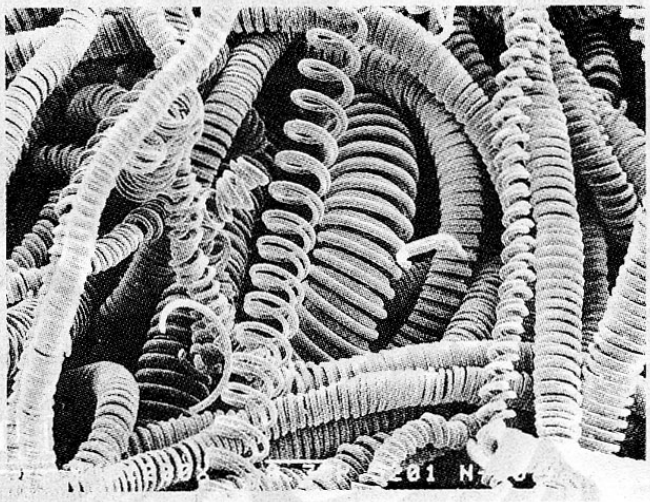

Figure 8. Irregular carbon coils.

shows the very regular-coiled double coils in which a single coil, having a large coil pitch, coiled on a single coil having a dense coil pitch. Fig. 10 shows two single coils which grow to an opposite direction each other and have an opposite coiling direction each other. If these two single coils entwine with each other with a coincided coiling axis, common double coils will be formed. Fig. 11 shows carbon coils having various interesting coiling patterns. Fig. 11(a) shows the paired double coils. Fig. 11 (b) shows a single coil in which

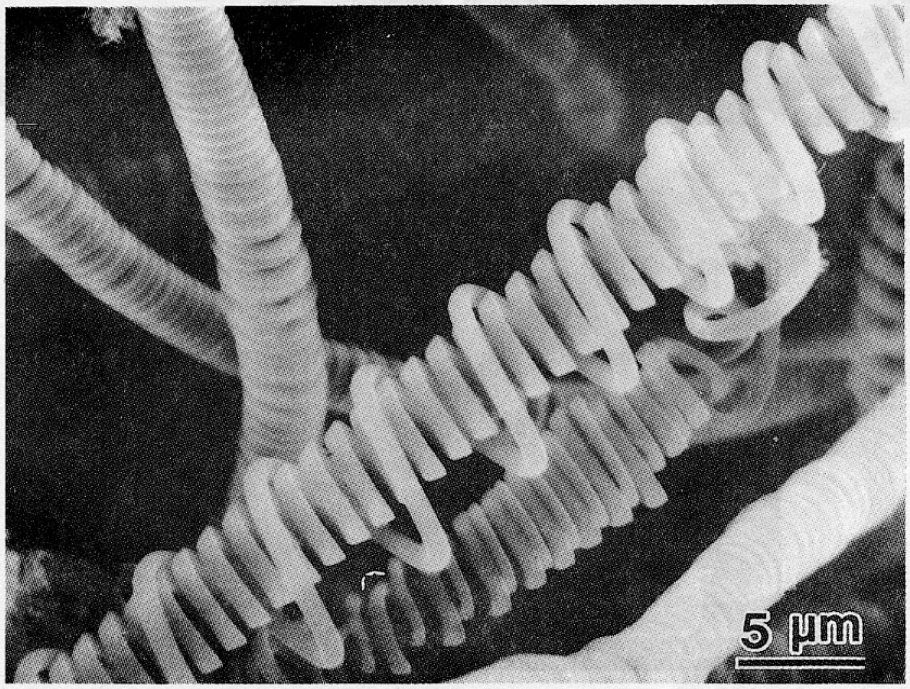

Figure 9. Double coils.

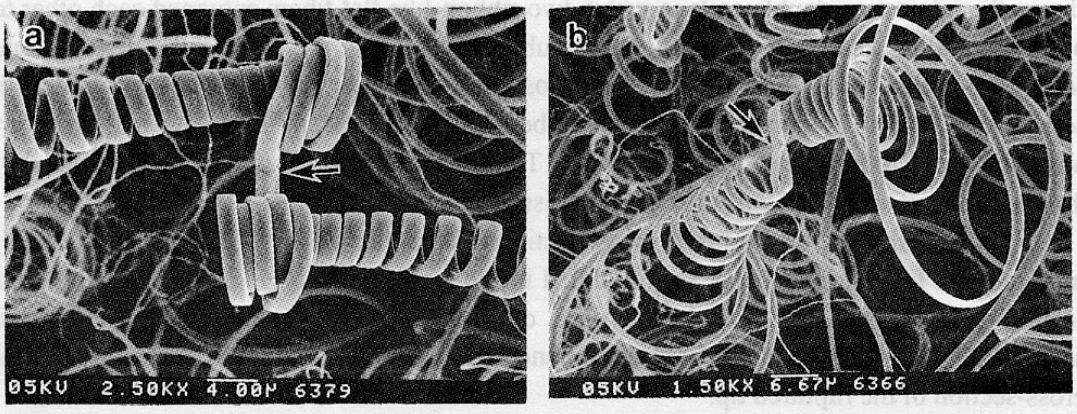

Figure 10. Paired single coils. Arrow indicates a catalyst grain.

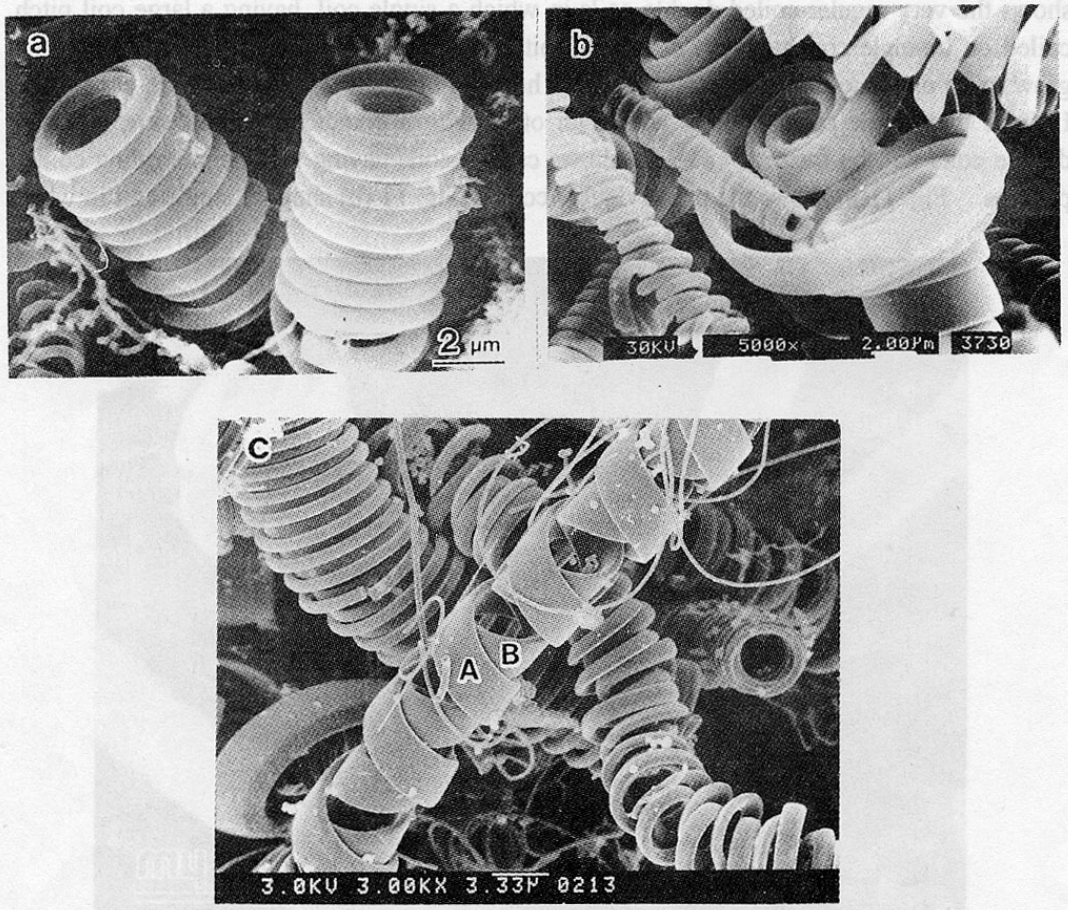

Figure 11. Various coiling morphologies.

a ribbon-like flat fiber coiled along the coil axis followed by a concentric coiling. Fig. 11(c) shows the interesting double coils in which two ribbon-like flat fibers entwined each other to opposite coiling direction to form one double coils. Fig. 12 shows the regular and concentric-coiled flat fibers. The outermost coil diameter is about 14μm which is comparable to that of commercial carbon fibers. These concentric coiling patterns were observed only on the ribbon-like flat fibers. These concentric coiling patterns are caused by the shape of a catalyst and the coiling mechanism.

Fig. 13 shows the ruptured cross section of the flat coils. The fiber is evenly ruptured and fine carbon grains are full filled in the cross section. Fig. 14 shows the cross section of the circular coils. In this case, one ruptured part is projected and another is hollowed. Fine hole, such as observed in nanotube, is not observed in the central part of the cross-section of the ruptured tip.

The very regular-coiled carbon coils with a flat fiber cross section and irregular-coiled carbon fibers with a circular fiber cross-section were commonly obtained with the EM field and without the EM field irrespective of the bias voltage, respectively.

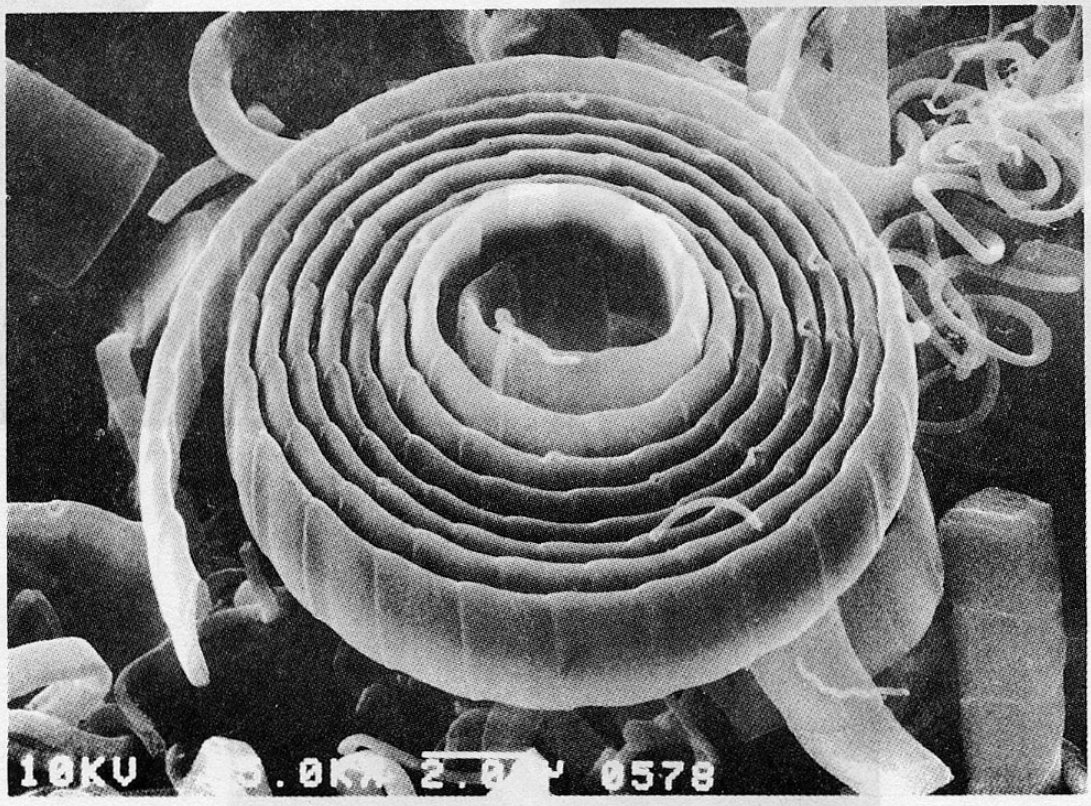

Figure 12. Concentric coil.

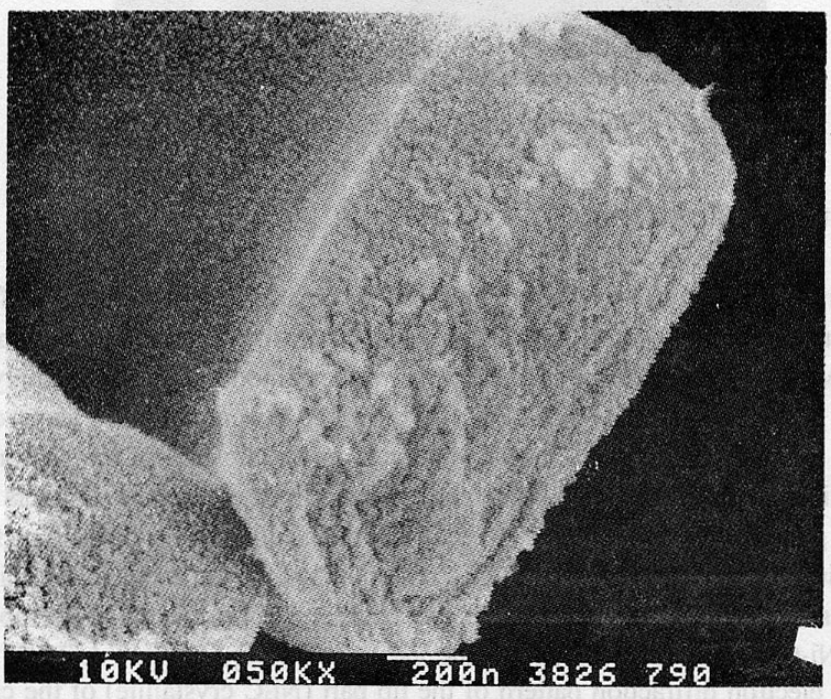

Figure 13. Ruptured cross section of a flat coil.

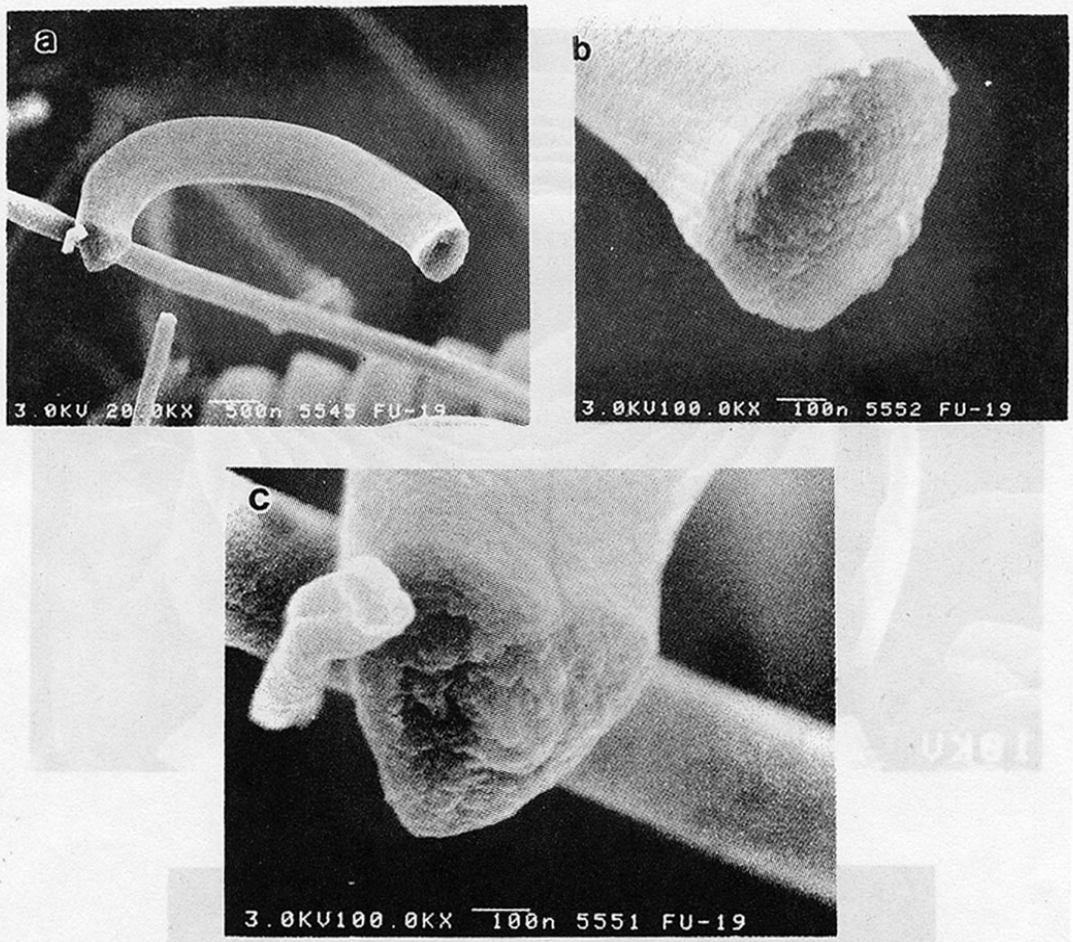

Fig.14. Ruptured cross sections of a circular coil.

4.3. Growth mechanism

It is very interesting to know why such peculiar coiling morphology can be formed and what is the growth mechanism of the carbon coils. Amelinckx et al. proposed a formation mechanism based on the concept of the spatial velocity hodograph for a catalytic grown helix-shaped graphite nanotube (17). Fig. 15 show the tip part of early stage of growing carbon coils. A brightened part (arrow) is always on the tip part of the carbon coils and form a loop-like shape, and this is a Ni catalyst grain. In other words, two fibers grew from a Ni catalyst grain present on the tip. The X-ray diffraction pattern of the structure in Fig. 15 is shown in Fig. 16. Some peaks of Ni_3C (rhombohedral) can be seen, in addition to that of amorphous carbon. This suggests that the brightened part located at the tip of carbon coils is the Ni_3C phase. Fig. 17 shows the various tip morphology. A TEM image and selected area electron diffraction pattern of the tip part (Ni_3C crystallite) of the carbon coils indicated by the arrow in Fig. 17 are shown in Fig. 18. Six spots can be seen in Fig. 18(b).

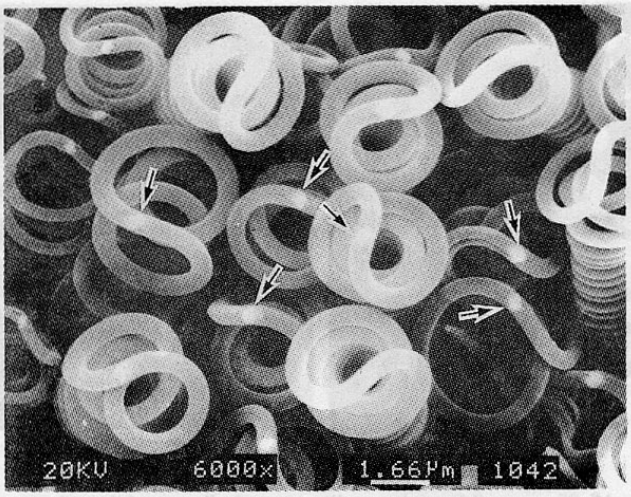

Figure 15. Tip part of the carbon coils of Initial growth stage. Reaction time: 30 s. Arrow indicates a catalyst grain.

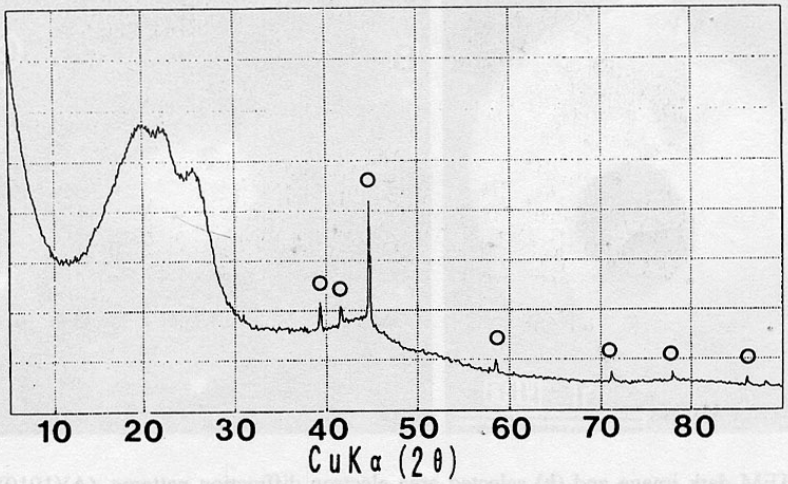

Figure 16. X-ray diffraction patterns of the carbon coils shown in Fig. 15. (○):Ni_3C (rhombohedral)

and spots A, B and C can be assigned to (1010), (0111) and (1101) of the Ni_3C phase, respectively. That is, the Ni_3C particle is a single crystal of Ni_3C. However, EDX analysis on the Ni_3C shows the presence of small amount of sulfur and oxygen on the surface of Ni_3C grain, while crystal phase of NiS_x, NiO_x, etc are not identified by XRD (35). It may be reasonably considered that, using Ni catalyst, actual catalyst is a Ni_3C single crystal grain on the surface of which Ni-C-S-O quartenary amorphous thin films are present. Figs. 19 and 20 show another type of the tip part of a coil obtained for 30 min reaction and the enlarged view. Four fibers grow from a Ni_3C catalyst grain (arrow) present in the central part of the

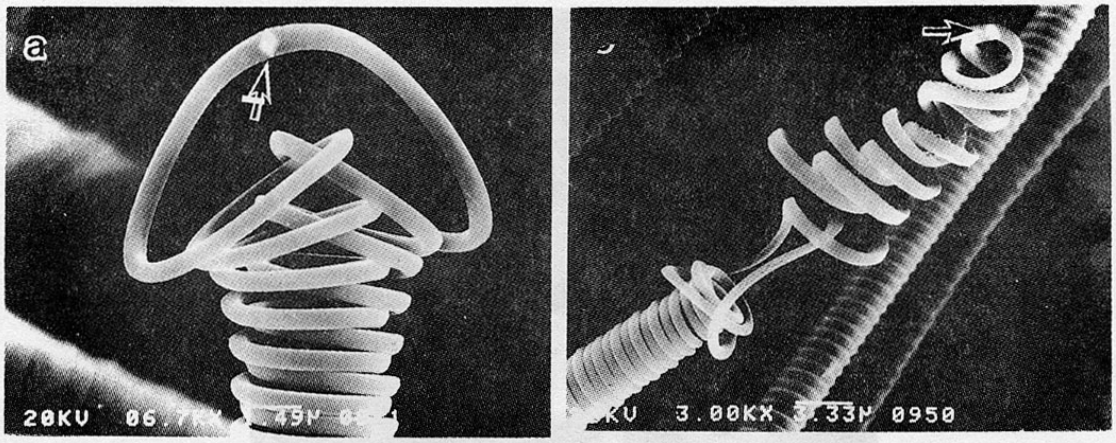

Figure 17. Tip part of the carbon coils. Arrow indicates a Ni catalyst grain.

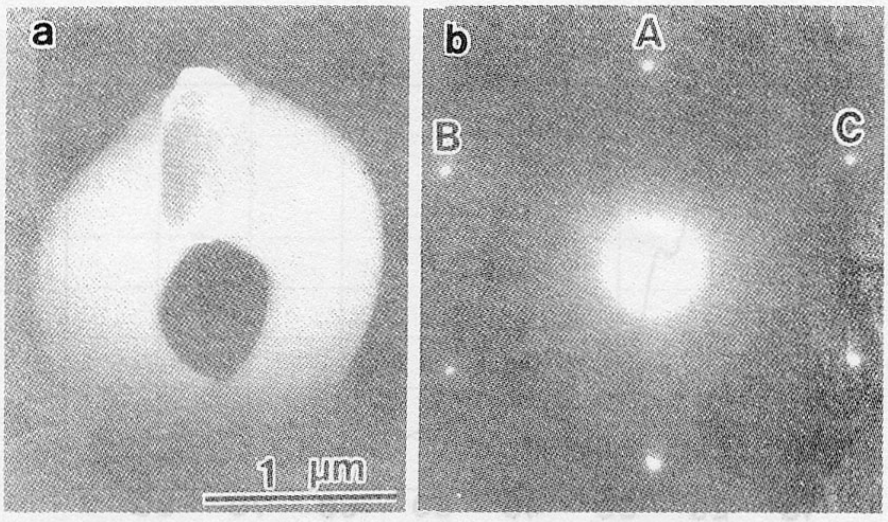

Figure 18. (a) TEM dark image and (b) selected area electron diffraction patterns. (A)(1010), (B)(0111), C(1101).

coil tip. The coil diameter decreases from about 35μm at the root part to 15μm at the tip (Fig. 20(a)). This Ni_3C grain is an exclusive growing point for carbon coils. It can be seen in Fig. 20(b) that six fibers, A, B, C, and A', B', C' grow from a Ni_3C grain (among which A and B and A' and B' coalesce together, respectively), and the six fibers coalesce to form two fibers, X and Y, and then form the double-coiled form. The postulated form of the Ni_3C grain embedded into the node of the six fibers is shown in Fig. 21, in which the Ni_3C grain is shown by a dashed cubic form outline, a~h. It may be reasonably considered that from the crystal face a-d-h-e, fiber A, from a-b-c-d, fiber B, from c-d-h-g, fiber C, from e-f-g-h, fiber A', from b-c-g-f, fibers B', and from a-b-f-e, fiber C' are forms. It was observed that fine

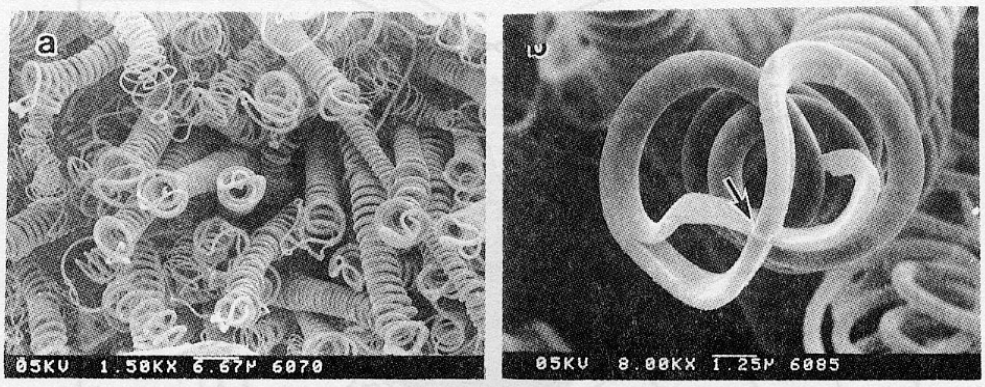

Figue 19. Tip part of the carbon coils.
Reaction time: 30 min. Arrow indicates a catalyst grain.

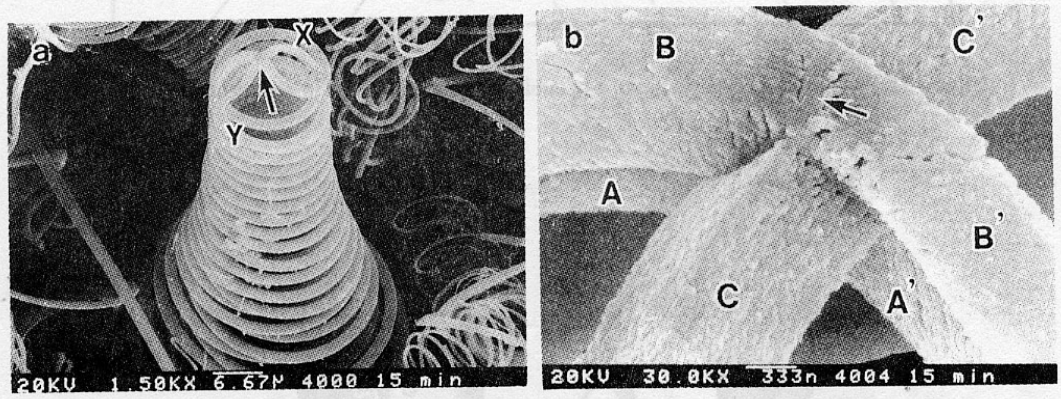

Figure 20. (a) Tip part of the regular coils and (b) enlarged view.
Reaction time: 30 min. X and Y: carbon coils, A~C and A'~C': carbon fibers, Arrow indicates a Ni catalyst grain.

and slender carbon deposits were concentrically oriented on the polished cross section of a carbon fiber that formed carbon coils, and the grain regions can apparently be divided into three parts (38).

A Ni single crystal plate with a (100), (111), (110) plane was used as a catalyst and substrate (29). The effect of the respective crystal face on the coil yield is shown in Table 1. It is observed that the coil yield differs based on the crystal faces, the yield order being (100)>(111)>(110). That is, there is large anisotropy of the catalytic effect of the respective crystal faces of the catalyst grain on the coil growth. From these results, we proposed the 3D-growth model of the carbon coils based on the catalytic anisotropy of the crystal faces of the catalyst grain (29, 35, 38, 52). Fig. 22(a) shows the growth model of the circular carbon coils. In this model, the order of the catalytic activity for the carbon deposition

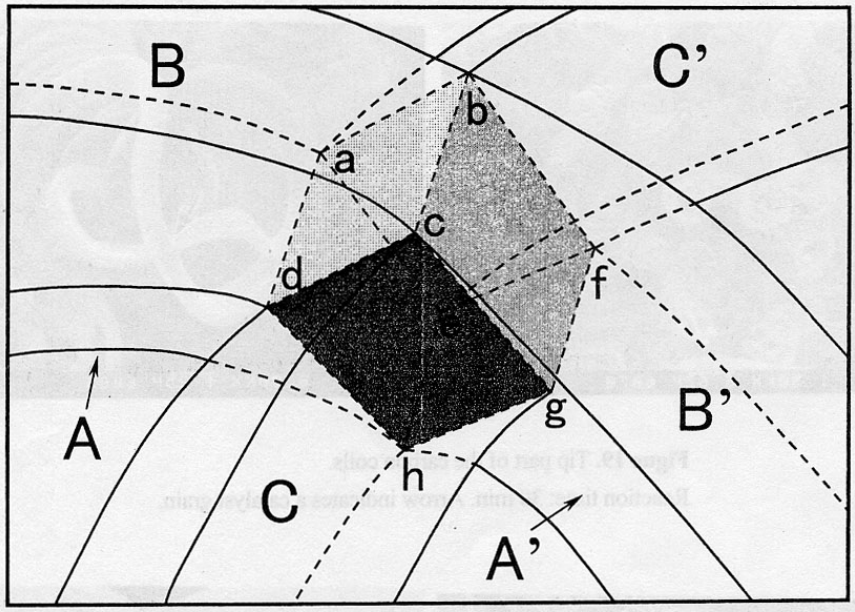

Figure 21. Postulated Ni catalyst grain. a-h: cubic Ni grain embedded in a node of six fibers.

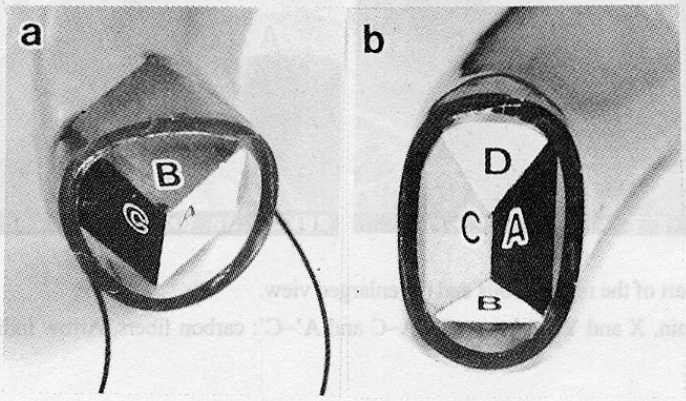

Figure 22. Schematic image of the growth mechanism of the carbon coils. (a) Circular coils, (b) flat coils. A-D: crystal faces.

among the three crystal faces is A>B>C, Basically, a carbon fiber is formed from the fine carbon grains deposited from the three crystal faces of A, B and C, and curl in such way that the carbon grains deposited from the crystal faces A and B are on the outer side of the coil, while the grains deposited from the crystal face C are inside. The coil diameter may be determined by the anisotropy of the carbon deposition between the crystal faces of A and C, and/or B and C, while the coil pitch by that of A and B. We have not yet identified the respective crystal faces as shown in Fig. 22. However, It may be reasonably considered

Table 1. Effects of Ni crystals (single- and poly-crystals) on the deposition of total carbon and coil yield.

	Crystal plane			Polycrystal. Ni plate
	Ni(100)	Ni(111)	Ni(110)	
Deposition rate of total carbon (mg/cm^2)	32	23	19	23
Coil Yield (mol.%)	10.2	6.7	3.2	4.8

that faces A, B, and C are (100), (111), and (110), respectively. Yang and Chen reported that for the carbon filament growth using the Ni catalyst pyrolysis of methane at 700°C, the most favored crystal face for graphite precipitation was Ni(111) followed by Ni(111)>(311)>(100)>(110) (53). The results obtained by us differ from the results of Yang and Chen only in that the order of (111) and (100) is reversed. The reason for this difference is not yet known. For the flat carbon coils, model (b), in which four crystal faces is concerned, can be adopted, and the coil diameter may be determined by the catalytic anisotropy between A and C, and coil pitch by B and D.

4.4. Preparation of micro-coils/micro-tubes of metal carbides and nitrides(54-59)

The carbon coils can be easily vapor phase metallized and/or nitided to form micro-coils of metal carbides and nitrides with full preservation of the coiling morphology of the carbon coils. Using very regular-coiled carbon coils without coil gap, micro-tube of MC_x/C(carbon coil)/MC_x~MC_x (MC_x:metal carbide) or MN_x/C/MN_x~MN_X (MN_x:metal nitride) can be obtained. These modification processes is shown in Fig. 23.

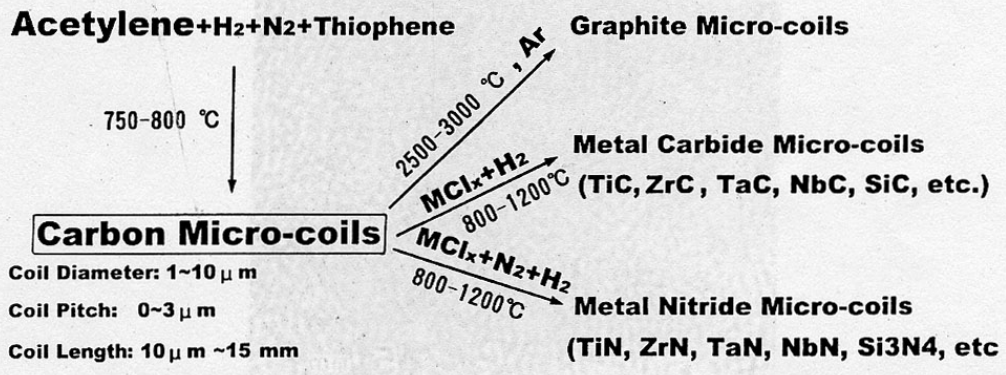

Figure 23. Modification routes of the carbon coils.

5. Properties

5.1. Composition and microstructure

The as-grown carbon coils is composed of 97.2~98.2 wt% C, 0.6~1.0 wt% O, 1.0~1.4 wt% H, 0.08~0.09 wt% S and 0.25 wt% Ni (27). XRD (Fig. 24), Raman spectra, and selected area electron diffraction patterns and TEM (Fig. 25) show that the as-grown carbon coils are an amorphous state while very fine films of the outermost surface is graphitized.

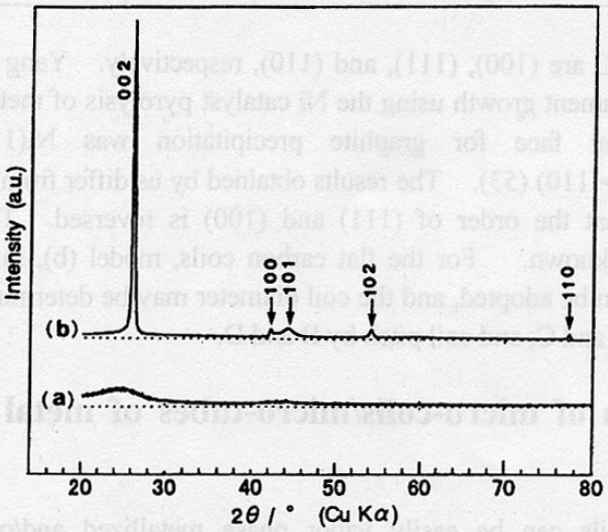

Figure 24. X-ray diffraction patterns. (a) As-grown carbon coils, (b) heat-treated carbon coils ("graphite coils") at 3000℃ for 6 hrs in $CO+CO_2$ atmosphere.

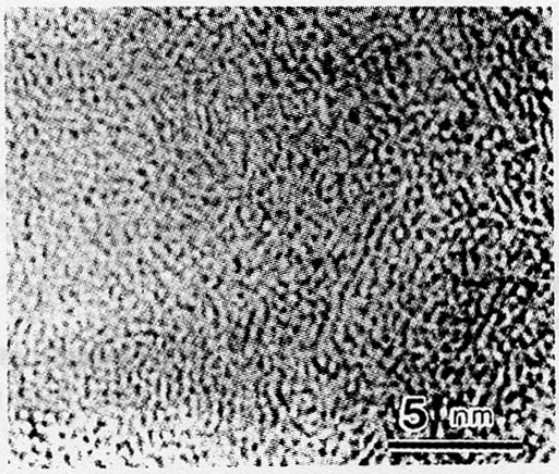

Figure 25. TEM image of the central part of the as-grown carbon coils.

5.2. Density, specific surface area, and pore size

Table 2 shows density, specific surface area, and average pore size. Using conventional electric heater for heating of reaction tube, that is, with EM field, and without bias voltage, density, specific surface area obtained with BET method, and average pore diameter of as–grown carbon coils was 1.7234 g/cm^3, 100~140 m^2/g, and 2~4 nm, respectively. The density increased by applying bias voltage, and was 1.8398 g/cm^3 with bias (DC 650V) (50). The density and specific surface area of the graphite micro-coils is 2.087~2.208 g/cm^3 and 6~8 m^2/g, respectively (60).

Table 2. Density, specific surface area an pore diameter of the as-grown carbon coils.

External EM field (AC, 60 Hz)	Bias voltage (V)	Density (g/cm^3)	Specific surface area (m^2/g)	Pore diameter (nm)
With	without	1.7234	100–140	3~4
	DC 650	1.8398		
	AC 1300	1.8018		
Without	without	1.7431	70–130	3~4
	DC 650	1.7978		
	AC 1300	1.7901		
Ref.	nanotube		240	–
(*carbon filters*)	VGCF	2.0817	20–30	
	PAN	1.7402	2–10	
	Pitch	2.0154	1–10	

5.3. Electric properties

The bulk (powder) electrical resistivity of the as-grown carbon coil decreases with increasing the bulk density, and is 1-10Ω· cm for 0.3 g/cm^3 and 0.1-0.2Ω· cm for 0.6 g/cm^3 as shown in Fig. 26(55,60). The resisitivity of the bulk carbon coils can be decreased steeply with the surface coating by carbon (61), TiC(55), TiN(56), ZrC(59), NbC(57), TaC(58), but not by graphitizing at high temperature heat treatment (57). The electrical resistance of a piece of flat carbon coils, as shown in Fig. 7, which is stepwise stretched up to 1.5 times of the original length, is shown in Fig. 27 (62). It can be seen that the resistance of the carbon coils increases stepwise by about one order of magnitude and saturated upon stretching. The stepwise increase of electrical resistance may be caused by the disconnection of electrical contact between helices and increase of inner stress during stretching. The electrical conductivity of the carbon coils along helix is 30~50 S/cm, which was estimated from the effective length of current path and cross section of the helix after stretching the coil.

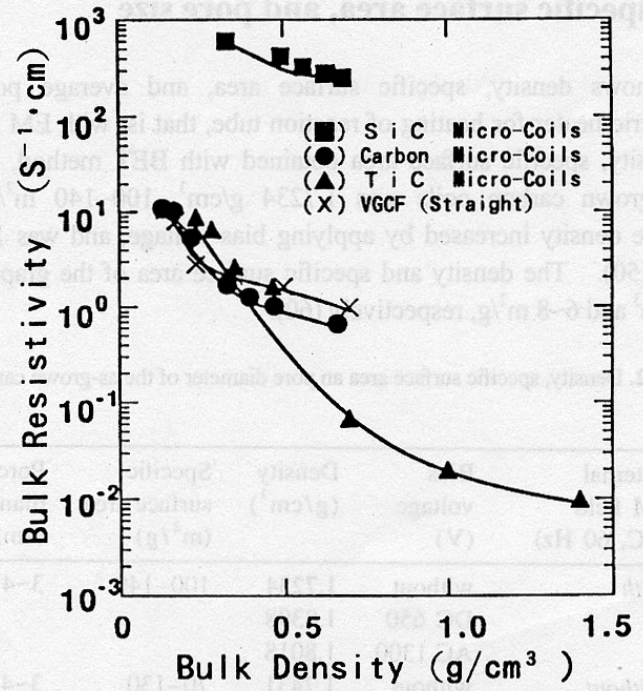

Figure 26. Dependence of electrical resistivity on the bulk density.

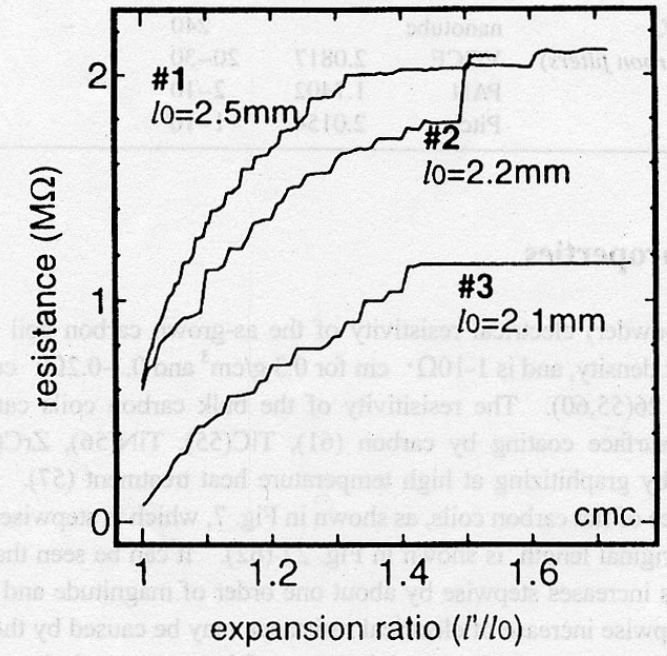

Figure 27. Dependence of resistance on the expansion ratio. l_0 : original length, l': expanded length.

This conductivity is rather small compared with multi-wall carbon nanotubes (63). Fig. 28 shows the current-voltage (i-v) characteristics of #4 before stretching and #5, which was stretched 1.5 times. The current shows super linear dependence on the applied voltage at high fields. The fact can be explained by heating of the coil by electrical power, because of the higher conductivity at higher temperature, or the high field effect. The abrupt decrease of current at the high field is due to burn out by the electrical breakdown. The temperature dependence of conductivity, which increased at high temperature, in an unstretched coil is analyzed based on various models of temperature dependent conductivities (64). As shown in Fig. 29, where plots are the relation of $\ln T^{1/2}\sigma$ against $T^{-1/4}$, the results indicates that one of the possible transport mechanism is the 3D variable range hopping model (65).

The electrical conductivities of the carbon coils under various gas atmospheres were examined, since π electron conductors may be affected by gases (66). The conductivity of a single coil increased by 5~20% upon evacuation for several minutes. Furthermore, the conductivity increased by 1~2% upon exposure to iodine (oxidative) gas for several minutes. On the other hand, upon exposure to ammonia (reductive) gas from the vacuum, the conductivity decreased nearly to the same value of the air atmosphere. However, the degree of conductivity was found to be small compared with the case of otherπconjugated systems such as conducting polymer.

The bulk electrical resistivity of the graphite coils is 10~0.1 $\Omega\cdot$ cm (60).

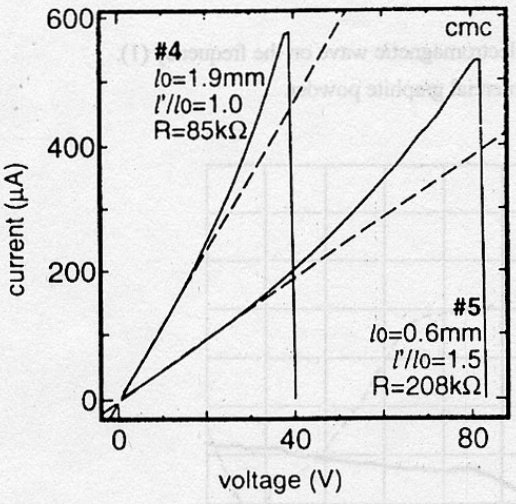

Figure 28. Current-voltage characteristics. (#4): before stretching, (#5): after stretched by 1.5 times.

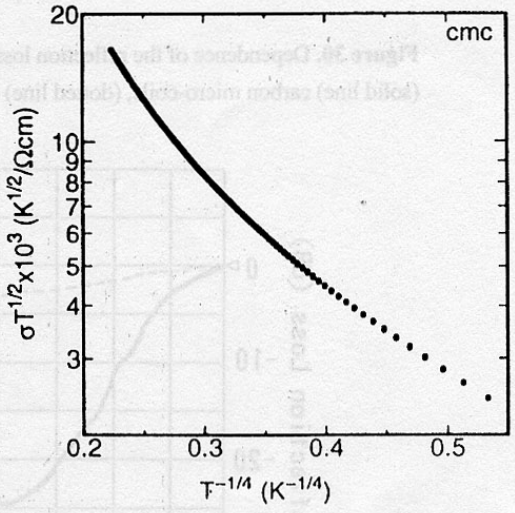

Figure 29. Temperature dependence of conductivity based on the 3D variable range hopping mode (61).

5.4. Electromagnetic properties

It is considered that the carbon coils is a promising candidate as a novel EM absorber, especially in the GHz range, because of its micro-coiling morphology. That is, the

micro-coiling morphology is the most effective and ideal one for the generation of inductive current by Faraday's Law resulting in absorption of EM wave. Actually, the carbon coils can absorbs EM wave in the GHz region without reflection (67). The as-grown carbon coils can strongly absorbed the EM wave of 13.9 GHz and 16.3 GHz, and the reflection loss is below –40dB as shown in Fig. 30 (68). The absorption region can be broadened by addition of other additives as shown in Fig. 31.

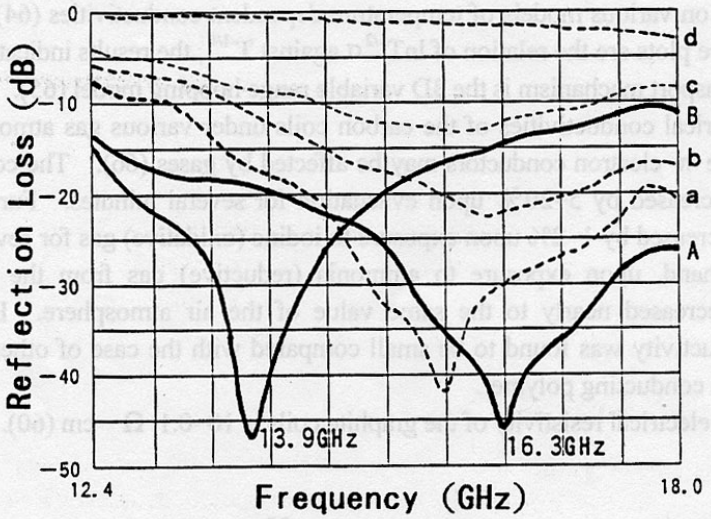

Figure 30. Dependence of the reflection loss of electromagnetic wave on the frequency (1). (solid line) carbon micro-coils, (dotted line) commercial graphite powder.

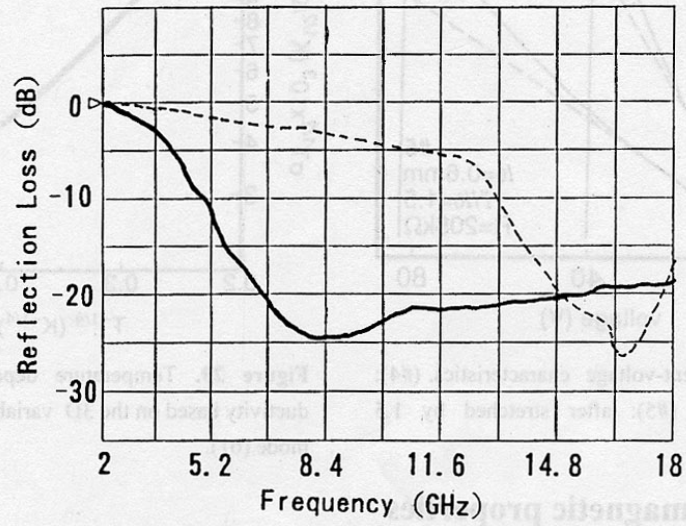

Figure 31. Dependence of the reflection loss of electromagnetic wave on the frequency (1). (—) carbon coils+ additives, (-----) carbon coils.

5.5. Magnetic properties (69)

Magnetoresistance of the as-grown and heat-treated carbon coils were measured in the magnetic field in the range from 0 to 12 Tesla at 290K. Magnetoresistance of the as-grown carbon coil does not change under strong magnetic field up to 12 Tesla. On the other hand, magnetoresistance in negative for specimens heat-treated at 1500°C, and 2000°C, and positive for specimens heat-treated at 2500°C. and 3000°C, The absolute value of magnetoresistance ratio {R(B)-R(0)}/R(0) increased with increasing magnetic field, and 40% under parallel magnetic field of 12T, and 5% at 5T and 14% at 12T under transverse field.

5.6. Mechanical properties (26,31,37,59,70)

The circular carbon coils with large coil diameter can expanded up to 4.5 ~15 times original coil length, while flat coils can be expanded elastically up to 1.5 times original length (26). The carbon coils expands linearly with increasing applied load. The rupture strength of the as-grown carbon coils is 42~114 MPa. The rigidity of the circular and flat as-grown carbon coils are 22~46 GPa and 22~33 GPa, respectively.

5.7. Chemical properties

The carbon coil becomes oxidize at about 450°C in air, and the weight significantly decreased with increasing temperature and burn out at 700°C as shown in Fig. 32 (71). On the other hand, the graphite micro-coils obtained by the heat treatment of as-grown carbon coils at 3000°C for 6 hrs in $CO+CO_2$ becomes oxidize at about 700°C in air. The oxidation behavior of the as-grown and heat-treated carbon coils are examined in details to improve the surface inertness and enhance the chemically active sites (70-72). The graphite coils is stable up to about 1200°C in Ar atmosphere. However, the graphite coils is

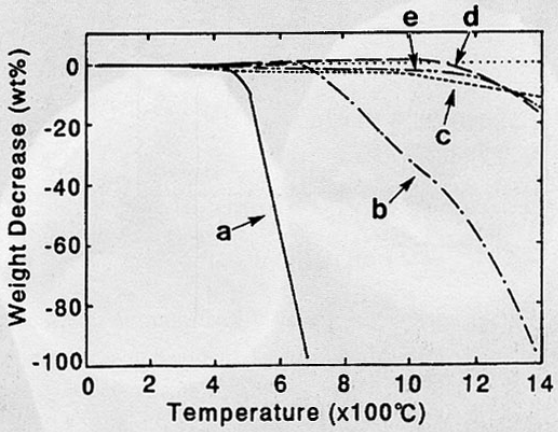

Figure 32. Effect of temperature on the weight decrease. Increasing temperature rate: 10°C/min by TG analyzer. (a) As-grown carbon coils, (b) graphite coils in air, (c) as-grown carbon coils in Ar, (d) graphite coils in Ar, (e) commercial graphite powder, (----) base line.

partially oxidized by the small amount of oxygen impurity included in Ar, at the contact part of two graphite layers in which large inner stress may be impressed to form amorphous state (71). Shibagaki et al. examined the partial oxidation characteristics of the surface of the carbon coils , under low O_2 flow rate at 450-820℃, to improve the surface chemical activities in details (72-74).

5.8. Thermal properties (31, 60)

The carbon coils can be heat-treated up to 3000℃ in $CO+CO_2$ atmosphere to form graphite coils with full reservation of the coiling morphology of the source as-grown carbon coils. The elasticity of the as-grown carbon coils is reduced by the heat-treatment and became brittle. The ruptured cross sections of the graphite coils obtained by the heat-treatment of the circular coils are shown in Fig. 33. The ruptured cross section of the

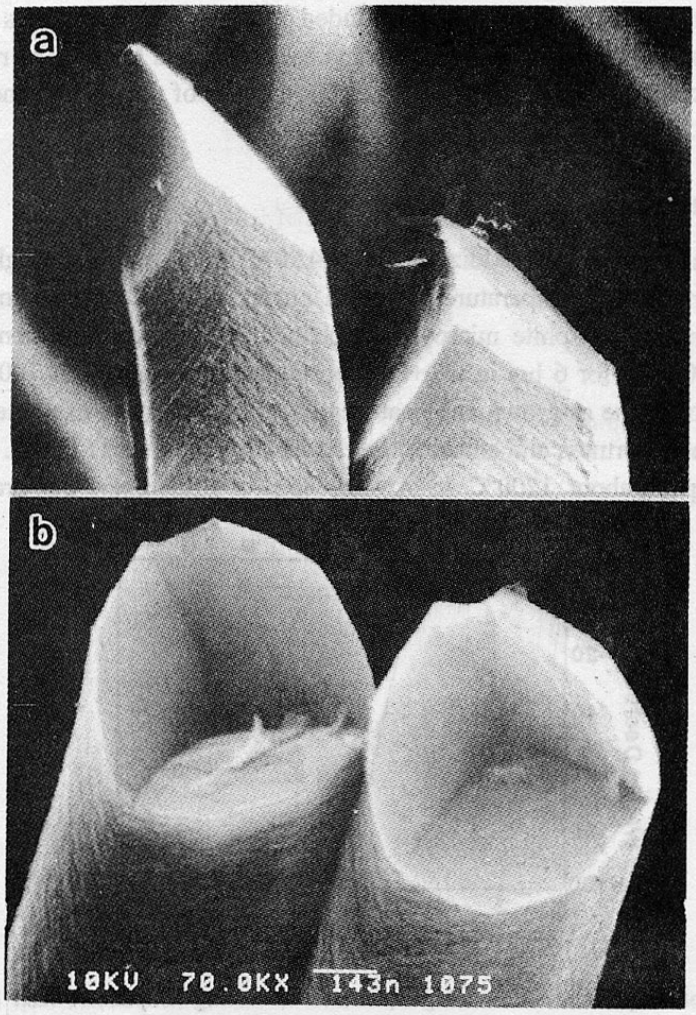

Figure 33. Ruptured tip part of the circular graphite coils exposed in air at 800℃ for 12 min. (a) Trigonal pyramid, (b) trigonal hollow.

two fibers, which form the coils, has either a trigonal pyramid-like form or negative pyramidal hollow. Fig. 34 shows the cross section of the graphite coils obtained by the heat treatment of flat coils following by partial oxidation. In this case, ruptured cross section has either roof-like extrusion or hollow. These characteristic patterns demonstrate the growth mechanism of the coils. Many distinct striations, declined at 40~50 deg against fiber axis, can be seen on the surface (Fig. 33(a)). Fig. 35 shows the TEM image of the tip part of the ruptured fiber. It can be seen that distinct graphite layers (d=0.339 nm) are developed with an inclination of 35~40 deg versus the fiber axis to form "herringbone" structure. Fig. 36 shows the model of the "herringbone" structure. The lattice parameter is a=0.2464 nm and c=0.6772 nm. The "c" value is slightly larger than the reported value for a graphite of 0.6714 nm while the "a" value is the same as that of graphite (a=0.2463 nm). Raman spectra shows that the graphite layers of the graphite coils are not more developed than the 100-200μm long VGCF. This may be caused by the presence of some disorders in the

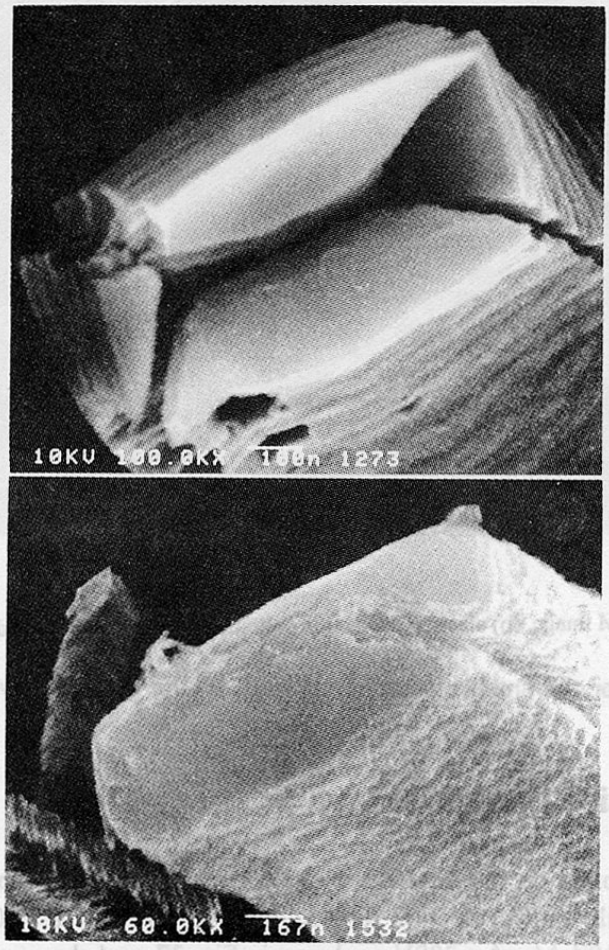

Figure 34. Ruptures tip part of the flat graphite coils exposed in Ar up to 1400°C.

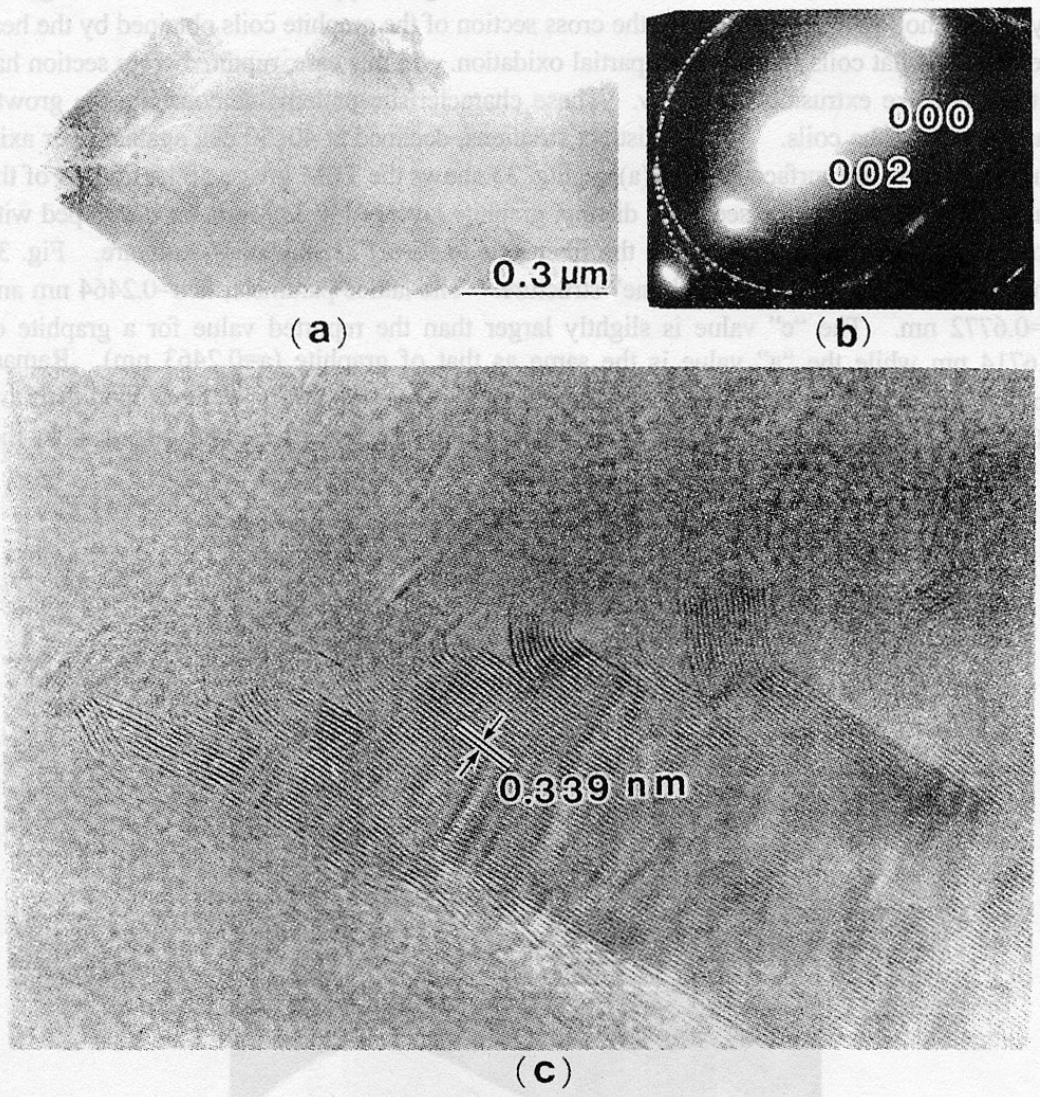

Figure 35. (a) TEM image, (b) electron diffraction patterns of the arrow in (a) and the lattice image.

graphite layers and/or the smaller submicron width of the graphite layers in the graphite coils.

5.9. Field emission properties

Pan et al. reported on the field emission properties of carbon tubule nanocoils (24). The carbon nanocoils shows the low turn-on field of 180V at a 130μm gap and high emission current of 10^{-3} A/cm^2 at 300V as shown in Fig. 37, and shows excellent stability of emission for over 250 hrs. Accordingly, the carbon nanocoils is expected as a novel attractive candidate for the fabrication of flat panel field emission display.

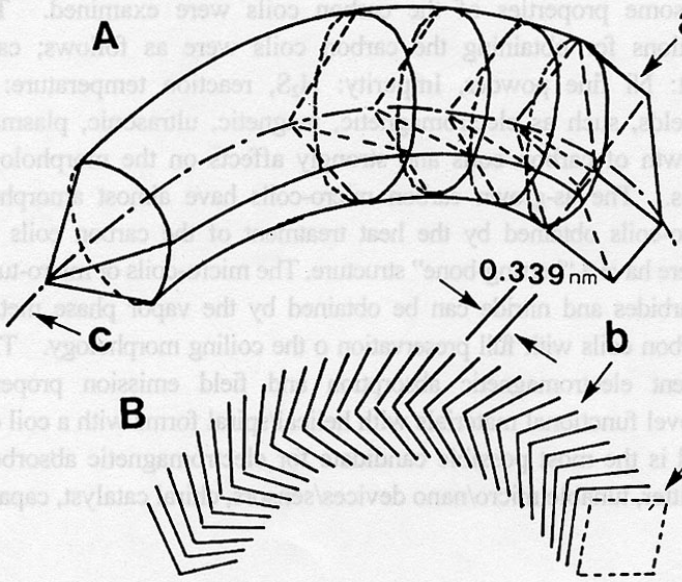

Figure 36. (A) Schematic 3D-model of the graphite coils with a herringbone structure and (B) 2D-model. Catalyst grain, (b) graphite layers, (c) fiber axis.

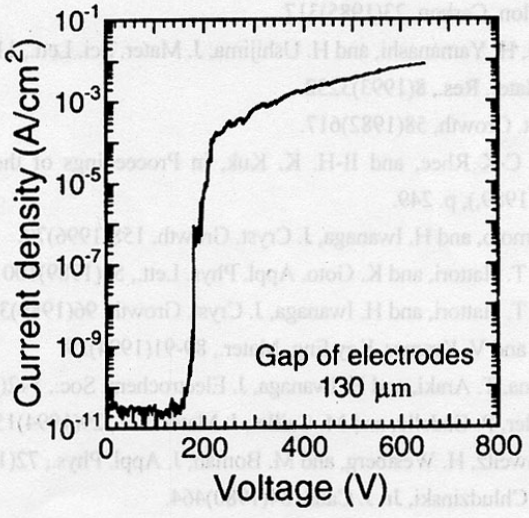

Figure 37. Curve of the emission current density vs applied voltage for a typical carbon nanocoils field emitter. The low turn-off voltage and high current density are obtained.

6. Conclusion

We have obtained the carbon micro-coils with a coil diameter ofμm~nm orders by the metal-catalyzed pyrolysis of acetylene, and the preparation conditions, morphology, growth

mechanism, and some properties of the carbon coils were examined. The optimum preparation conditions for obtaining the carbon coils were as follows; carbon source: acetylene, catalyst: Ni fine powder, Impurity: H_2S, reaction temperature: 750~800°C Various energy fields, such as electromagnetic, magnetic, ultrasonic, plasma fields, etc., accelerate the growth of carbon coils and strongly affects on the morphology and some physical properties. The as-grown carbon micro-coils have almost amorphous structure. The graphite micro-coils obtained by the heat treatment of the carbon coils at 3000°C in $CO+CO_2$ atmosphere have a "herring-bone" structure. The micro-coils or micro-tubes of various transition metal carbides and nitride can be obtained by the vapor phase metalizing and/or nitriding of the carbon coils with full preservation o the coiling morphology. The carbon coil shows the excellent electromagnetic absorption and field emission properties. Carbon micro-coils is a novel functional materials with helical/spiral forms with a coil diameter of μ m~nm orders, and is the most possible candidate for electromagnetic absorbers, hydrogen absorber, field emitter, tunable micro/nano devices/sensors, chiral catalyst, capacitors, energy convertors, etc.

References

1. W.R. Davis, R.J. Slawson, and G.R. Rigby, Nature, 171(1953)756.
2. J. Calszka and M.H. Back, Carbon, 22(1984)141.
3. M. Audier and M. Coulon, Carbon, 23(1985)317.
4. Y. Okada, K. Takeuchi, H. Yamanashi, and H. Ushijima, J. Mater. Sci. Lett., 11(1992)1715.
5. N.M. Rodoriguez, J. Mater. Res., 8(1993)3232.
6. A. Addamiano, J. Cryst. Growth, 58(1982)617.
7. T-K kang, S-D Park, C-K Rhee, and II-H. K. Kuk, in Proceedings of the 6th Japan-Asia Ceramic seminar (Kobe, Japan, 1989,), p. 249.
8. S. Motojima, T. Hamamoto, and H. Iwanaga, J. Cryst. Growth, 158(1996)79.
9. S. Motojima, S. Ueno, T. Hattori, and K. Goto, Appl. Phys. Lett., 54(1989)1001.
10. S. Motojima, S. Ueno, T. Hattori, and H. Iwanaga, J. Cryst. Growth, 96(1989)383.
11. U. Vogt, H. Hofmann, and V. Kramer, Key Eng. Mater., 89-91(1994)29.
12. S. Motojima, T. Yamana, T. Araki, and H. Iwanaga, J. Electrochem. Soc., 142(1995)3141.
13. P. Gleize, M.C. Schouler, P. Gadelle, and M. Caillet, J. Mater. Sci., 29(1994)1575.
14. S. Johansson, J-A. Schweitz, H. Westberg, and M. Boman, J. Appl. Phys., 72(1992)5956.
15. R.T. K. Baker and J.J. Chludzinski, Jr, J. Catal. 64(1980)464.
16. K. Hernadi, A. Fonseca, J.B. Nagy, D.Bernaerts, and A.A. Lucas, Carbon, 34(1996)1249.
17. S. Amelinckx, X.B. Zhang, D. Bernaerts, X.F. Zhang, V. Ivanov, and J.B. Nagy, Science, 265(1994)635.
18. W. Li, S. Xie, W. Liu, R. Zhao, Y. Zhang, W. Zhou, G. Wang, and L. Qian, J. Mater. Sci., 34(1999)2745.
19. J.M. Mao and S.S. Xie, J. Mater. Sci. Lett., 18(1999)1151.
20. M. Zhang, Y. Nakayama, and L. Pan, Jpn. J. Appl. Phys., 39(2000)L1242.
21. H. Takikawa, M. Yatsuki, R. Miyano, M. Nagayama, T. Sakakibara, S. Itoh, and Y. Ando, Jpn. J. Appl.

Phys., 39(2000)5177.
22. F. Cesar, J-O. Bovin, L.R. Wallenberg, G. Karlsson, L.K.L. Falk and T. Oku, J. Mater. Res., 15(2000)1857.
23. S. Ihara and S. Itoh, Carbon, 33(1995)931.
24. L. Pan, T. Hayashida, M. Zhang, and Y. Nakayama, Jpn. J. Appl. Phys., 40(2001)L235.
25. S. Motojima, M. Kawaguchi, K. Nozaki, and H. Iwanaga, Appl. Phys. Lett., 56(1990)321.
26. S. Motojima, M. Hirata, and H. Iwanaga, J. Chem. Vapor Deposition, 3(1994)87.
27. S. Motojima, Y. Itoh, S. Asakura, and H. Iwanaga, J. Mater. Sci., 30(1995)5049.
28. S. Motojima, S. Asakura, M. Hirata, and H. Iwanaga, Mater. Sci. Eng., B34(1995)L9.
29. S. Motojima, S. Asakura, T. Kasemura, S. Takeuchi, and H. Iwanaga, Carbon, 34(1996)289.
30. S. Motojima, T. Hamamoto, N. Ueshima, Y. Kojima, and H. Iwanaga, Electrochem. Soc. Proc, 97-25(1997)433.
31. S. Motojima, Y. Kojinma, T. Hamamoto, N. Ueshima, and H. Iwanaga, Electrochem. Soc. Proc., 97-39(1997)595.
32. S. Motojima, X. Chen, T. Kuzuya, W.In Hwang, M. Fujii and H. Iwanaga, J. de Phys., IV,9(1999)Pr8-445.
33. X Chen and S. Motojima, Carbon, 37(1999)1817.
34. X. Chen and S. Motojima, J. Mater. Sci., 34(1999)5519.
35. X. Chen, T. Saito, M. Kusunoki and S. Motojima, J. Mater. Res., 14(1999)4329.
36. S. Motojima, X. Chen, W. In Hwang, T. Kuzuya, M. Kohda, and Y. Hishikawa, Electrochem. Soc. Proc., 2000-12, p. 379.
37. X. Chen, Y. Hishikawa, W. In Hwang, T. Kuzuya and S. Motojima, Electrochem. Soc. Proc., 2000-12, p. 385.
38. S. Motojima and X. Chen, J. Appl. Phys., 85(1999)3919.
39. R.T.K. Baker, M.A. Baker, P.S. Harris, F.S. Feates, and R.J. Waite, J. Catal., 26(1972)51.
40. R.T.K. Baker and J. Waite, J. Catal., 37(1975)101.
41. W.R. Davis, R.J. Slawson, and G.R. Rigby, Trans. Brit. Ceram. Soc., 56(1957)67.
42. J. Caluszka and M.H. Back, Carbon, 22(1984)141.
43. L.S. Labo and D.L. Trimm, J. Catal., 29(1973)15.
44. R.T.K. Baker and R.J. Waite, J. Catal., 37(1975)101.
45. S. Motojima and X. Chen, J. Mater. Sci., 34(1999)3581.
46. O. Feron, F. Langlais, and R. Naslain, Electrochem. Soc. Proc., 97-25(1997)49.
47. D.B. Murphy, R.W. Carroll, and J.E. Klonowski, Carbon, 35(1997)1819.
48. W. Benzinger, A. Becker, and K.J. Hullinger, Carbon, 34(1996)957.
49. W-In Hwang, X. Chen, M. Kohda, and S. Motojima, Mater. Technol., 18(2000)263.
50. W. In-Hwang, X. Chen, T. Kuzuya, K. Kawabe, and S. Motojima, Carbon, 38(2001)565.
51. W. In-Hwang, X. Chen, K. Kawabe, and S. Motojima, J. Mater. Eng. B, (accepted)
52. M. Kawaguchi, K. Nozaki, S. Motojima and H. Iwanaga, J. Cryst. Growth, 118(1992)309.
53. R.T. Yang and J.P. Chen, J. Catal., 115(1989)52.
54. S. Motojima, S. Kagiya and H. Iwanaga, J. Mater. Sci., 31(1996)4641.
55. S. Motojima, S. Yang, X. Chen and H. Iwanaga, J. Mater. Sci., 34(1999)5989.
56. S. Motojima, W.-In Hwang, X. Chen and H. Iwanaga, J. Electrochem. Soc., 147(2000)1228.

57. S. Motojima, W. In Hwang, and X. Chen., Mater. Res. Bull., 35(2000)1517.
58. S. Motojima, W. In-Hwang, and H. Iwanaga, J. Mater. Sci., 36(2001)673.
59. S. Motojima, H. Asano and H. Iwanaga, J. Euro. Ceram. Soc., 16(1996)989.
60. X. Chen, W-In Hwang, S. Shimada, M. Fujii, H. Iwanaga and S. Motojima, J. Mater. Res., 15(2000)808.
61. X. Chen, S. Motojima and H. Iwanaga, Carbon, 37(1999)1825.
62. K. Kaneto, M. Tsuruta, and S. Motojima, Synthetic Mater., 103(1999)2578.
63. K. Kaneto, G. Sakai and W.Y. Cho, and Y. Ando, Synthetic Mater., 103(1999).
64. N.F. Motto, Metal Insulator Transition, Taylor & Francis Ltd. London (1974)37.
65. A.J. Epstein, H. Rommelmann, R. Bigelow, W. Gibson, D.M. Hoffmann and D.B. Tanner, Phys. Lev. Lett., 50(1983)1866.
66. H. Inokuchi and M. Sano, Ed. By Shirakawa and T. Yamane, Gousei Kagaku, Kagakudojin, (1980)p127.
67. V.K. Varadan, private communication to S. Motojima.
68. S. Motojima and H. Iwanaga, Kinou Zairyou, 17(1997)1.
69. M. Fujii, M. Matsui, S. Motojima, and Y. Hishikawa, Proc. ICCG-13, (Kyoto, 2001).
70. S. Motojima, M. Kawaguchi, K. Nozaki, and H. Iwanaga, Carbon, 29(1991)379.
71. W-In Hwang, T. Kuzuya, H. Iwanga, and S. Motojima, J. Mater. Sci., 36(2001)971.
72. K. Shibagaki and S. Motojima, Mater. Technol., 39(2001)400.
73. K. Shibagaki, S. Motojima and M. Hashimoto, Mater. Technol., 18(2001)411.
74. K. Shibagaki and S. Motojima, Mater. Technol., 19(2001) (in press).